2020 IEEE/RSJ International Conference on Intelligent Robots and Systems (IROS)
October 25-29, 2020, Las Vegas, NV, USA (Virtual)

The Omega Turn: A Biologically-Inspired Turning Strategy for Elongated Limbless Robots

Tianyu Wang[1,*], Baxi Chong[2,*], Kelimar Diaz[2], Julian Whitman[1], Hang Lu[2], Matthew Travers[1], Daniel I. Goldman[2], Howie Choset[1]

***Abstract*— Snake robots have the potential to locomote through tightly packed spaces, but turning effectively within unmodelled and unsensed environments remains challenging. Inspired by a behavior observed in the tiny nematode worm *C. elegans*, we propose a novel in-place turning gait for elongated limbless robots. To simplify the control of the robots' many internal degrees-of-freedom, we introduce a biologically-inspired template in which two co-planar traveling waves are superposed to produce an in-plane turning motion, the *omega turn*. The omega turn gait arises from modulating the wavelengths and amplitudes of the two traveling waves. We experimentally test the omega turn on a snake robot, and show that this turning gait outperforms previous turning gaits: it results in a larger angular displacement and a smaller area swept by the body over a gait cycle, allowing the robot to turn in highly confined spaces.**

I. Introduction

Snake robots are capable of maneuvering through tightly packed and confined spaces, making them appealing for use in search and rescue or industrial maintenance [1]–[3]. Due to their unconventional mode of locomotion, body undulation, much research on snake robot locomotion has focused on designing cyclic motions (gaits) and managing the interactions with the surrounding environment [4]–[6]. Most often, planar locomotory behaviors have been achieved by varying joint angles according to a traveling wave, and most prior work has focused on forward motion. In this paper, we consider turning gaits, as we believe the ability to reorient plays a critical role in agile snake robot locomotion, especially in complex, cluttered, unstructured and highly damped environments which constrain maneuverability.

Hirose [7] first introduced a turning behavior for snake robots by augmenting body waves with a constant offset in curvature. By regulating this constant offset, the robot was able to steer, a method we refer to as "offset turning." Subsequent work demonstrated the effectiveness of the offset turn in two-dimensional snake robot locomotion problems [8]. Dai et al. [9] used techniques from geometric mechanics, the application of differential geometry to rigid body motion, to design a gait that enables in-place turning, a method we refer to as a "geometric turn." Both of these in-plane turning behaviors are achieved by propagating a single traveling wave along the body of the robot and modulating the parameters of the traveling wave [10]. To gain a richer set of behaviors, we propose to move beyond the single-wave template while maintaining a low-dimensional means of coordinating the many joints on the body.

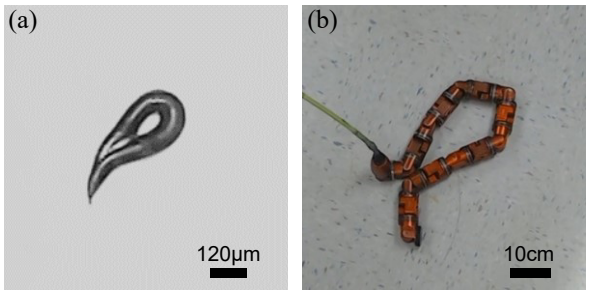

Fig. 1: In this work we present a biologically-inspired turning gait to enable a snake robot to reorient in confined spaces. (a) The omega (Ω) shaped turning behavior of the nematode worm *C. elegans*. (b) The omega turn executed with a snake robot.

We turn to biology to find examples of effective turning behaviors. The gait presented in this paper is inspired by a motion commonly found in *Caenorhabditis elegans*, a millimeter-scale nematode worm often used as a model organism [11], [12]. Within the literature, the turning motion is called an *omega turn* because during the course of turning the anterior end of the body (head) sweeps near the posterior end of the body (tail), inscribing an "Omega" (Ω) shape (Fig. 1a).

Stephens et al. [12] showed that the postures of *C. elegans* locomoting on agar can be described with four total principal components (PCs). The first three PCs corresponded to forward motion (PC 1 and 2) and turning (PC 3). Interestingly, the forward motion PCs and turning PC were found to have different spatial wavelengths. Inspired by this finding, we develop a template in which the snake robot's joint angles follow a superposition of two coplanar traveling waves with different wavelengths. The two wave components can be defined in terms of their resulting motions when isolated from each other. The first wave results in forward motion, and is of the same form as previously proposed planar undulatory motions [13]. The second wave causes the "omega" shape on the robot's backbone and, when combined properly with the first wave, results in in-place turning.

The main contribution of this paper is to take recourse to tools found in geometric mechanics to determine the optimal parameter selection in the omega turn gait template to max-

*These authors contributed equally

[1]Tianyu Wang, Julian Whitman, Matthew Travers and Howie Choset are with Carnegie Mellon University, Pittsburgh, PA 15213, USA. {tianyuw2@andrew, jwhitman@andrew, mtravers@andrew, choset@cs}.cmu.edu

[2]Baxi Chong, Kelimar Diaz, Hang Lu, and Daniel I. Goldman are with Georgia Institute of Technology, Atlanta, GA 30332, USA. {bchong9, kelimar.diaz, hang.lu}@gatech.edu, daniel.goldman@physics.gatech.edu

imize turning displacement on the robot. Then, we compare the performance of the gait through numerical simulations and robot experiments (Fig. 1b). We also compare the omega turn gait with turning gaits from prior work [7], [9]. Our experiments quantitatively demonstrate the benefits of using this method of turning over the others: it creates a larger angular displacement per gait cycle than is possible with previous methods, and it sweeps a smaller area, allowing it to be effective in confined or obstacle-dense spaces.

We note that at this point, it is no longer entirely accurate to call our robot a "snake" given that its behavior is inspired by nematodes. However, we will continue to follow the historical precedent of denoting these elongated mechanisms as snake robots.

II. Related Work

A. Offset turn

A common form of locomotion displayed by biological snakes and reproduced by snake robots is lateral undulation, a planar motion characterized by a travelling wave moving along the backbone. A mathematical description of this motion is known as the *serpenoid curve* [7], in which the system's (snake or snake robot) joints follow a traveling wave,

$$\theta_i(t) = A\sin\left(2\pi\omega t + 2\pi k\frac{i}{N}\right) + \kappa, \tag{1}$$

where i is the index of the joint, N the total number of joints, θ_i the ith joint angle, A the wave amplitude, and t the time. ω is the temporal frequency, which determines how fast the wave propagates along the backbone. k is the spatial frequency, which determines the wavelength of the serpentine shape on the robot's backbone.

The parameter κ in (1) governs the locomotion direction in the undulation gait: forward motion occurs when κ is zero, and a combination of forward and turning, the offset turn, occurs when κ is non-zero. The offset turn is used widely in snake robot implementations since it can be easily achieved using the undulation gait template [14].

B. Geometric turn

An engineered (not biologically-inspired) but surprisingly effective turning gait for snake robots was discovered by Dai et al. using tools from geometric mechanics [9]. The geometric mechanics framework divides the system's configuration space into the position space and the shape space: the position space contains the world-frame position and orientation of the system, and the shape space contains the internal configuration (shape) of the system [15]. Within this framework, the serpenoid curve was described as a weighted sum of sine and cosine modes,

$$\theta_i = \begin{bmatrix}\sin(2\pi k\frac{i}{N}) & \cos(2\pi k\frac{i}{N})\end{bmatrix}\begin{bmatrix}r_1 & r_2\end{bmatrix}^T \tag{2}$$

where r serves as shape space parameters that describe the amplitude and phase of the wave in (1). k, i, and N keep the same definitions with those in (1) [16]. Given this shape parameterization and an environment interaction model, a *local connection* $\boldsymbol{A}(r)$ can be constructed to map the changes in shape parameters to changes in body position by

$$\xi = \boldsymbol{A}(r)\dot{r}, \tag{3}$$

where $\xi = [\xi_x\ \xi_y\ \xi_\theta]^T$ denotes the forward, lateral, and rotational body velocities. The local connection matrix, $\boldsymbol{A}$, can be numerically derived by force and torque balances in overdamped environments, such as Coulomb friction environments. Prior work [17] showed that numerically derived local connections using kinetic Coulomb friction can accurately model motion on flat hard ground.

Each row of the local connection $\boldsymbol{A}$ corresponds to a body velocity component. Given the local connection evaluated at discrete location in the shape space, the collection of each row of the local connections forms a connection vector field over the target shape space. Thus each of the body velocities can be computed as the dot product of the corresponding connection vector field and the shape velocity $\dot{r}$. Furthermore, a periodic gait can be represented as a closed path in the shape space. The displacement resulting from a gait, $\partial\chi$, can be approximated by

$$\begin{bmatrix}\Delta x\\ \Delta y\\ \Delta\theta\end{bmatrix} = \int_{\partial\chi}\boldsymbol{A}(r)dr. \tag{4}$$

According to Stokes' Theorem, the line integral along a closed path $\partial\chi$ is equal to the surface integral of the curl of $\boldsymbol{A}(r)$ over the surface enclosed by $\partial\chi$:

$$\int_{\partial\chi}\boldsymbol{A}(r)dr = \iint_{\chi}\nabla\times\boldsymbol{A}(r)dr_1dr_2, \tag{5}$$

where χ is the surface enclosed by $\partial\chi$. The curl of the connection vector field, $\nabla\times\boldsymbol{A}(r)$, is referred to as the height function. The three rows of the vector field $\boldsymbol{A}(r)$ can thus produce three height functions in the forward, lateral and rotational direction, respectively.

By experimentally determining the local connections over the whole shape space, Dai et al. [9] used the height function in the rotational direction to identify a turning gait which produced maximum turning displacement per gait cycle under this single-wave template. We refer to this turning method as the "geometric turn."

III. The Two-wave Gait Family and Omega Turns

A. Turning behavior in C. elegans

While thought of as simple organism, *C. elegans* exhibits behaviors and performances in complex environments not seen in robots. One of these behaviors is the worm's turning strategy, known as omega (Ω) turns [11]. These worms generate a high curvature bend such that the head touches body and outlines an omega (Ω) shape, allowing the worms to turn in place. The worms were observed to use *omega* turns to explore unknown environments, avoid navigational bias, and to escape painful external stimuli [19]–[21]. Note that the *omega* turn can produce effective turning performance in a variety of environments with different drag anisotropy. These turns are advantageous when navigating and traversing complex heterogeneous terrain that the worms encounter throughout their lifetime. Stephens et al. [12] showed that the *C. elegans* kinematics during free crawling can be described with more than two principal components. Two principal components are observed to characterize a traveling wave for

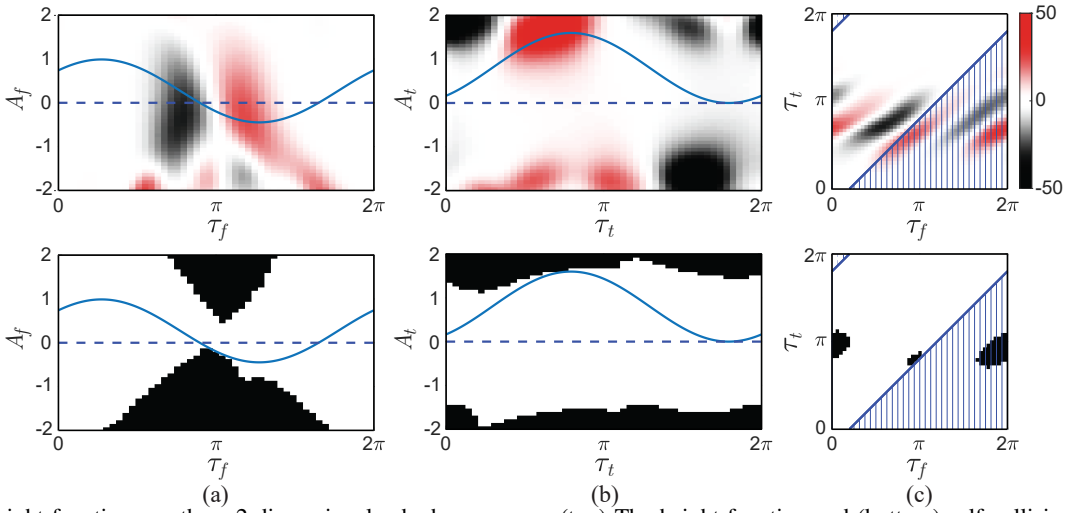

Fig. 2: The height functions on three 2-dimensional sub-shape spaces. (top) The height function and (bottom) self-collision region on the shape space (a) $\{[\tau_f\ A_f], \tau_f \in S^1, A_f \in \mathbb{R}^1\}$ (b) $\{[\tau_t\ A_t], \tau_t \in S^1, A_t \in \mathbb{R}^1\}$ (c) $\{[\tau_f\ \tau_t], \tau_f \in S^1, \tau_t \in S^1\}$. The red and black colors represent the positive and negative values of the height function on the top figures. The black regions in the bottom figures represents the shapes that lead to self-collision. The blue curve shows the gait paths f_1, f_2 and f_3, designed to maximize the surface integral while not passing through the collision regions. The surface integrals in (a) and (b) is the integral of surface enclosed by the gait path and the dashed line; in (c) is the integral of surface enclosed in the lower right corner (shadow by solid line) minus the surface enclosed in the upper left corner (shadow by dashed line) [18].

the forward motion. Surprisingly, another principal component is observed to drive the turning motion. This suggests that a single traveling sinusoidal wave is not sufficient to describe turning behaviors. Based on this observation, and our further examination of the motions of *C. elegans*, we propose that omega turns can be represented by two planar sinusoidal waves with different spatial frequencies. This is a higher-dimensional gait representation than those in most prior snake robot gaits, but remains structured and low-dimensional while enabling a richer set of behaviors.

B. A family of two-wave turning gaits

Inspired by the body waves on the *C. elegans*, in this section we describe a template for a family of in-plane turning gaits. The template is a superposition of two coplanar traveling sinusoidal waves: a *forward wave* and a *turning wave*, with joint angles prescribed by

$$\begin{aligned}\theta_i(t) =& A_f(t)\sin\left(2\pi\omega t + 2\pi k_f\frac{i}{N}\right) + \\ & A_t(t)\sin\left(2\pi\omega t + 2\pi k_t\frac{i}{N} + \psi\right),\end{aligned} \tag{6}$$

where ω, i, t, and N keep the same definitions as in (1). k_f, $A_f(t)$ are the spatial frequency and time-varying amplitude of the forward wave. k_t, $A_t(t)$ are the spatial frequency and amplitude of the turning wave. ψ is the phase offset between the two waves. Note that when $k_t = 0$, (6) becomes

$$\theta_i(t) = A_f(t)\sin\left(2\pi\omega t + 2\pi k_f\frac{i}{N}\right) + \kappa(t), \tag{7}$$

where $\kappa(t) = A_t(t)\sin(2\pi\omega t + \psi)$. The offset turn (1) can therefore be considered a special case of the two-wave gait family. Additionally, when $k_t = k_f$, (6) can be rewritten,

$$\theta_i(t) = r_1(t)\sin\left(2\pi k_f\frac{i}{N}\right) + r_2(t)\cos\left(2\pi k_f\frac{i}{N}\right), \tag{8}$$

where $r_1(t) = A_f(t)\cos(2\pi\omega t) + A_t(t)\cos(2\pi\omega t + \psi)$ and $r_2(t) = A_f(t)\sin(2\pi\omega t) + A_t(t)\sin(2\pi\omega t + \psi)$. (8) is equivalent to the geometric turn as in (2), therefore the geometric turn is also a special case of the two-wave gait family.

C. The omega turn gait

So far, we have noted that the turning motion of *C. elegans* can be described by a superposition of two traveling waves, and found that the two-wave turning template in (6) contains two previous turning methods. However, these facts do not inform us what values of wave parameters to use, or how to synchronize the two waves for our given robot, which has a different geometry and environment interaction model than the nematode worm.

We turn to geometric tools to optimize turning displacement per gait cycle subject to self-collision avoidance for our robot model. For the remainder of this work, we fix the spatial frequency of the forward wave at $k_f = 1.5$ to keep consistent with the forward wave observed in worms, and study turning gaits within the two-wave family.

We apply the hierarchical geometric framework [22] to optimize omega turn gaits. Specifically, we construct a four-dimensional shape space $[A_f, \tau_f, A_t, \tau_t]^T$, such that

$$\theta_i = A_f\sin\left(\tau_f + 2\pi k_f\frac{i}{N}\right) + A_t\sin\left(\tau_t + 2\pi k_t\frac{i}{N}\right). \tag{9}$$

The gait path in the shape space can then be described as: $f : t \mapsto [A_f, \tau_f, A_t, \tau_t]^T, t \in S^1$.

Some internal shapes lead to self-collision, which we disallow in our robot implementation. We construct a collision map on the shape space and add the constraints that the gait path of f cannot pass through the self-collision region.

Note that τ_f and τ_t are cyclic. In this way, we can simplify the gait path in the four-dimensional shape space to three simple functions in the two-dimensional sub-shape spaces [22]: $f_1 : \tau_f \mapsto A_f$, $f_2 : \tau_t \mapsto A_t$, and $f_3 : \tau_f \mapsto \tau_t$ ($f_3^{-1} : \tau_t \mapsto \tau_f$). Given any two simple functions, we can

reduce the shape space dimension to two. For example, given f_1, and f_3, (9) becomes

$$\begin{aligned}\theta_i =& f_1 \circ f_3^{-1}(\tau_t) \sin\left(f_3^{-1}(\tau_t) + 2\pi k_f \frac{i}{N}\right) \\ &+ A_t \sin\left(\tau_t + 2\pi k_t \frac{i}{N}\right) = \theta_i(A_t, \tau_t).\end{aligned} \tag{10}$$

Given (10), we can reduce the original shape space to $\{[\tau_t \ A_t], \tau_t \in S^1, A_t \in \mathbb{R}^1\}$, from which we can numerically calculate the height function to optimize for f_2. Similarly, given f_1 and f_2, the height functions on $\{[\tau_f \ \tau_t], \tau_f \in S^1, \tau_t \in S^1\}$ can be numerically calculated; given f_2 and f_3 the height functions on $\{[\tau_f \ A_f], \tau_f \in S^1, A_f \in \mathbb{R}^1\}$ can be numerically calculated. In the optimization, we iteratively optimize the three simple functions f_1, f_2 and f_3 until a local maximum in turning angle per gait cycle is reached.

For computational simplicity, we reduce the search space of f_1, f_2 and f_3 by prescribing the functions below:

$$\begin{aligned} f_1 &: \tau_f \mapsto A_f, A_f = a_f(\gamma + \sin(\tau_f + \phi_f)), \\ f_2 &: \tau_t \mapsto A_t, A_t = a_t(1 + \sin(\tau_t + \phi_t)). \\ f_3 &: \tau_t \mapsto \tau_f, \tau_f = \tau_t + \psi, \end{aligned} \tag{11}$$

The converged height functions and gait paths are shown in Fig. 2. It may be possible to obtain slightly higher performing gaits by using more complex functions to describe the trajectory through shape space, e.g. as in [23]. However, simpler functions of paths through the shape space are correspondingly easier to optimize and execute on the robot, while still nearing the performance from such complex functions.

IV. Experiments

We tested the omega turn gait in both a simple numerical simulation and on a physical snake robot. To compare the performance of the omega turn with other spatial frequencies within the two-wave template, we tested a series of gaits with varying $k_t \in [0, 1.5]$, including the offset turn ($k_t = 0$) and the geometric turn ($k_t = 1.5$).

A. Numerical simulation

We performed a numerical simulation to predict turning performance for a given set of wave parameters. Assuming quasi-static motion, the trajectory of the robot can be determined by integrating the ordinary differential equation throughout one period [16]. The angular displacement can thus be determined over one gait cycle. The results are shown in Section V.

B. Snake robot experiment

We carried out experiments with a snake robot composed of sixteen identical actuated joints. The joints are arranged such that the axes of rotation of neighboring modules are torsionally rotated 90° relative to each other. A low-level PID controller embedded in each joint of the robot controls the actuators to follow the joint angle set points. Since the turning gaits presented here are two-dimensional, i.e., the motion of the robot is planar, only half of the joints were controlled following (6), while every other joint angle was set to zero.

Experiments were conducted on flat, smooth, hard ground and in a two-dimensional artificial indoor obstacle-rich peg board environment. We assume the ground reaction forces are given by kinetic Coulomb friction [17]. For each gait parameter setting tested, we conducted three trials. In each trial, we commanded the snake robot to execute three gait cycles. We tracked the motion of the snake robot via eight reflective markers affixed along the backbone of the robot and an OptiTrack motion capture system.

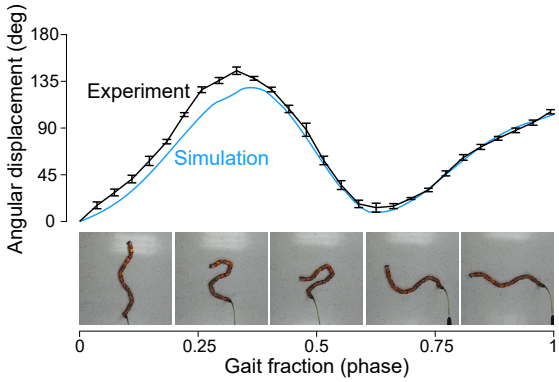

Fig. 3: Time evolution of the angular displacement in the simulation and the robot experiments during an omega turn. Each point represents the average over three trials, and the error bars indicate the standard deviation. A sequence of video frames of the robot depicts the time evolution of the robot's body shape in 10 seconds.

V. Results

A. Simulation-experiment comparison during an omega turn

We found that a turning wave spatial frequency of $k_t = 1.0$ enabled the snake robot to turn most effectively. Therefore we refer to the two-wave gait with $k_t = 1.0$ as the omega turn, although other gaits with similar parameters result in similar body shapes. We measured the rotation angle of the snake robot during a complete gait cycle using the positions tracked by the motion capture system, and compare them to the trajectory found in the numerical simulation. We observe close agreement between the simulation and the experimental results, as shown in Fig. 3. There, a sequence of video frames depicts the time evolution of the robot's body shape. During the progression of an omega turn, the body first folds so that the anterior end of the body comes close to the posterior end of the body to form an omega (Ω) shape, and then unfolds to complete the turn. A visual comparison between the omega turning behavior of *C. elegans* and the omega turning motion of the snake robot can be found in the supplementary video.

B. Turning speed

Next, we compared the turning speed of the omega turn gait with other gaits in the two-wave gait family defined by (6). With fixed temporal frequency $\omega = 2.5$, we tested a range of gaits by sampling the spatial frequency of the turning wave k_t from $[0, 1.5]$ with a 0.25 stride, and conducted three trials for each gait. Notice that the gait with $k_t = 0$ is the offset turn, $k_t = 1.0$ is the omega turn, and $k_t = 1.5$ is the geometric turn. Fig. 4 shows the results of the angular displacement per gait cycle for each gait. The simulation and experiment results share similar trends, in which the omega turn outperforms other gaits in the turning gait family. The average angular displacement of the omega turn is $105.7^\circ \pm$

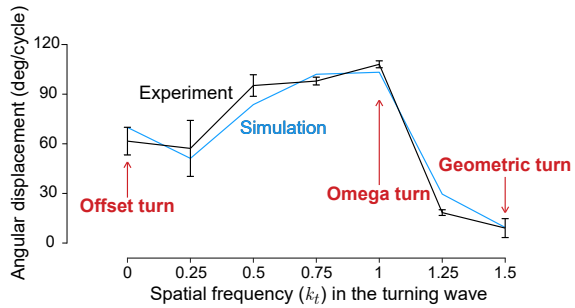

Fig. 4: The angular displacement for the turning gaits over a range of turning wave spatial frequencies (k_t) on flat ground. Error bars indicate the standard deviation. Omega turns have the largest angular displacement both in simulation and reality.

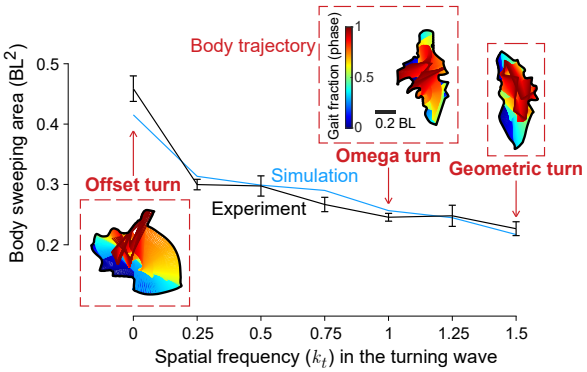

Fig. 5: The area swept by the body for the turning gaits with varied turning wave spatial frequency k_t. The results are normalized by the robot body length squared (BL^2). Error bars indicate the standard deviation. The time evolution of robot's configurations executing the designed gaits over a period are shown in the red dashed boxes, where the gait fraction is indicated by colors from the beginning (blue) to the end (red). The geometric turn has the lowest swept area due to the fact that its net rotation is also low. The omega turn has the smallest swept area per degree angular displacement achieved over the cycle.

2.1°, while the average angular displacement of the offset turn and the geometric turn are 61.6° ± 8.4° and 9.0° ± 5.7°, respectively. The larger angular displacement per gait cycle implies that the omega turn is a more efficient turning strategy on flat ground. Examples of the experiments can be found in the supplementary video.

Note that the offset turn we tested in these comparisons was optimized with a time-variant offset as per (7). The optimized time-varying offset turn consistently outperformed the constant offset turn, and so the latter was not included in our comparisons.

C. Area swept by the body

To evaluate the potential effectiveness of these turning gaits within confined spaces, we compared the body swept area per gait cycle. The body swept areas were obtained by computing the convex hull of all points the tracked positions on the robot passed through over the course of a cycle. These areas were averaged over three trials, and normalized by the body length squared (BL^2). Fig. 5 depicts the body swept areas for the gaits tested. The body swept area for the omega turn is 0.25 ± 0.01 BL^2, while the body sweeping area for the offset turn is 0.46 ± 0.02 BL^2. As we have showed in Section V-B, turning gaits with $k_t = 1.25$ and $k_t = 1.5$ (the geometric turn) are the least effective on flat ground.

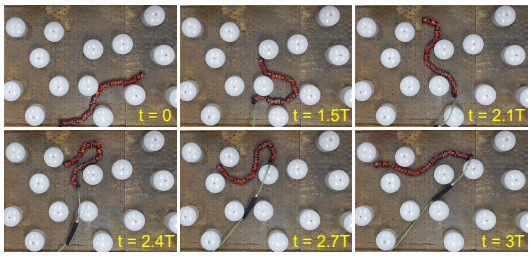

Fig. 6: A sequence of video frames of the robot executing omega turns in a randomly arranged planar peg board. The omega turn produced 51.3° angular displacement per gait cycle on the robot on average. Here time t is measured in terms of complete gait cycle period T.

The swept areas for these settings are small because they did not generate as much turning motion on the robot. The omega turn has the smallest swept area per degree angular displacement achieved over the cycle. Smaller swept areas imply that the omega turn reduces the possibility of the robot colliding with obstacles, potentially allowing the robot to turn in narrower spaces.

D. Experiments in a confined space

To test the potential effectiveness of omega turning gaits within confined environments, we performed the omega turn, geometric turn, and offset turn gaits in a two-dimensional artificial indoor obstacle-rich environment, a randomly arranged peg board. The controls in these experiments are open-loop; no feedback control policy is applied.

The omega turn gaits exhibit effective turning behaviors in the planar peg board. An example of successful omega turning motions on the peg board is shown in Fig. 6. The robot was able to generate 51.3° ± 27.3° angular displacement per gait cycle on average over three trials. Note that the turning performance is highly dependent on the distribution of the obstacles, therefore the standard deviation of the turning angle is relatively large. The offset turn and the geometric turn gaits performed poorly, generating far less turning motion within the pegs, 8.6° ± 5.1° and 4.7° ± 3.2° angular displacement per gait cycle, respectively. A comparison video of three gaits in the same environment can be found in the supplementary video. These preliminary test shows that the omega turn is the most promising among the tested turning gaits within confined spaces.

VI. Discussion

With the help of the geometric mechanics gait optimization framework, we were able to design gaits for limbless elongated mechanisms based on the motions of the nematode worm using the proposed two-wave template. We can qualitatively decompose the optimal omega turn into three stages:

1) Enter the turning mode by decreasing the amplitude of the forward wave and increasing the amplitude of the turning wave.
2) Execute turning by reversing the direction of the forward wave (negative amplitude) and further increasing the amplitude of the turning wave.
3) Exit the turning mode by increasing the amplitude of the forward wave and decreasing the amplitude of the turning wave.

VII. Conclusion

In this paper, we presented a novel biologically-inspired turning strategy for snake robots, based on the omega turns observed in the tiny nematode worm *C. elegans*. We found through simulation and robot experiments that the omega turn strategy allows the robot to turn effectively within a small area. The small area swept by the body may reduce the possibility of colliding with obstacles in heterogeneous environments. Therefore, our turning strategy offers promise for snake robots locomoting in complex, confined and highly damped environments.

We found that the performance of the geometric turn on the flat ground is worse than its performance in granular media reported by [9]. While we have not yet conducted a full analysis of the various turning gaits in different environments, our initial observations of the omega turn in granular media indicate that it may perform comparably to the geometric turn. This suggests that the geometric turn is not as robust to different environment types as the omega turn. One direction for our future work is thus in testing these gaits in different environments, including granular media and unstructured/confined spaces. Similarly, we may perform experiments on the *C. elegans* to measure the impact that different environments have on their turning strategies.

Our new two-wave gait template is a superposition of two traveling sinusoidal waves in the same plane, in contrast to the existing single-wave planar template. One drawback to this approach is that there are additional parameters in the template, making it more difficult to optimize, plan, and control these gaits. However, we believe that the significant performance gains are worth the few additional parameters. A continued avenue for our research is to study the trade-off between the performance of the agile snake robot motion and the dimensionality of the motion templates. Further, we plan to move beyond open-loop gaits to integrate the two-wave template into reactive control strategies [4], [6].

Our prior work on snake robots has drawn biological inspiration primarily from biological snakes. This work suggests that other organisms with elongated body structures may provide valuable insights. Many animals with different anatomy, morphology, and physiology rely on undulatory locomotion to traverse myriad environments [24]. While undulatory locomotion is a relatively simple form of locomotion, its presence across scales is indicative that it is remarkably robust. Using limbless robots, we can test biologically-inspired templates and gain gain insight on control strategies used by undulators across scales. Perhaps robots of the future may draw the best properties from all limbless locomotors.

References

[1] J. Whitman, N. Zevallos, M. Travers, and H. Choset, "Snake robot urban search after the 2017 mexico city earthquake," in *2018 IEEE international symposium on safety, security, and rescue robotics (SSRR)*. IEEE, 2018, pp. 1–6.

[2] A. Masayuki, T. Takayama, and S. Hirose, "Development of "souryu-iii": connected crawler vehicle for inspection inside narrow and winding spaces," in *2004 IEEE/RSJ International Conference on Intelligent Robots and Systems (IROS)(IEEE Cat. No. 04CH37566)*, vol. 1. IEEE, 2004, pp. 52–57.

[3] S. A. Fjerdingen, P. Liljebäck, and A. A. Transeth, "A snake-like robot for internal inspection of complex pipe structures (piko)," in *2009 IEEE/RSJ International Conference on Intelligent Robots and Systems*. IEEE, 2009, pp. 5665–5671.

[4] M. J. Travers, J. Whitman, P. E. Schiebel, D. I. Goldman, and H. Choset, "Shape-based compliance in locomotion." in *Robotics: Science and Systems*, 2016.

[5] A. A. Transeth, R. I. Leine, C. Glocker, K. Y. Pettersen, and P. Liljebäck, "Snake robot obstacle-aided locomotion: Modeling, simulations, and experiments," *IEEE Transactions on Robotics*, vol. 24, no. 1, pp. 88–104, 2008.

[6] T. Wang, J. Whitman, M. Travers, and H. Choset, "Directional compliance in obstacle-aided navigation for snake robots," in *2020 American Control Conference (ACC)*, 2020, pp. 2458–2463.

[7] S. Hirose, "Biologically inspired robots," *Snake-Like Locomotors and Manipulators*, 1993.

[8] C. Ye, S. Ma, B. Li, and Y. Wang, "Turning and side motion of snake-like robot," in *IEEE International Conference on Robotics and Automation, 2004. Proceedings. ICRA'04. 2004*, vol. 5. IEEE, 2004, pp. 5075–5080.

[9] J. Dai, H. Faraji, C. Gong, R. L. Hatton, D. I. Goldman, and H. Choset, "Geometric swimming on a granular surface." in *Robotics: Science and Systems*, 2016.

[10] R. J. Full and D. E. Koditschek, "Templates and anchors: neuromechanical hypotheses of legged locomotion on land," *Journal of experimental biology*, vol. 202, no. 23, pp. 3325–3332, 1999.

[11] N. A. Croll, "Components and patterns in the behaviour of the nematode *Caenorhabditis elegans*," *Journal of zoology*, vol. 176, no. 2, pp. 159–176, 1975.

[12] G. J. Stephens, B. Johnson-Kerner, W. Bialek, and W. S. Ryu, "Dimensionality and dynamics in the behavior of *C. elegans*," *PLoS computational biology*, vol. 4, no. 4, 2008.

[13] M. Saito, M. Fukaya, T. Iwasaki, *et al.*, "Modeling, analysis, and synthesis of serpentine locomotion with a multilink robotic snake," *IEEE control systems magazine*, vol. 22, no. 1, pp. 64–81, 2002.

[14] A. Mohammadi, E. Rezapour, M. Maggiore, and K. Y. Pettersen, "Maneuvering control of planar snake robots using virtual holonomic constraints," *IEEE Transactions on Control Systems Technology*, vol. 24, no. 3, pp. 884–899, 2015.

[15] J. E. Marsden and T. S. Ratiu, *Introduction to mechanics and symmetry: a basic exposition of classical mechanical systems*. Springer Science & Business Media, 2013, vol. 17.

[16] R. L. Hatton and H. Choset, "Nonconservativity and noncommutativity in locomotion," *The European Physical Journal Special Topics*, vol. 224, no. 17-18, pp. 3141–3174, 2015.

[17] J. M. Rieser, C. Gong, H. C. Astley, P. E. Schiebel, R. L. Hatton, H. Choset, and D. I. Goldman, "Geometric phase and dimensionality reduction in locomoting living systems," *arXiv preprint arXiv:1906.11374*, 2019.

[18] C. Gong, Z. Ren, J. Whitman, J. Grover, B. Chong, and H. Choset, "Geometric motion planning for systems with toroidal and cylindrical shape spaces," in *ASME 2018 Dynamic Systems and Control Conference*. American Society of Mechanical Engineers Digital Collection, 2018.

[19] L. C. Salvador, F. Bartumeus, S. A. Levin, and W. S. Ryu, "Mechanistic analysis of the search behaviour of *Caenorhabditis elegans*," *Journal of The Royal Society Interface*, vol. 11, no. 92, p. 20131092, 2014.

[20] O. D. Broekmans, J. B. Rodgers, W. S. Ryu, and G. J. Stephens, "Resolving coiled shapes reveals new reorientation behaviors in *C. elegans*," *Elife*, vol. 5, p. e17227, 2016.

[21] A. Mohammadi, J. B. Rodgers, I. Kotera, and W. S. Ryu, "Behavioral response of *Caenorhabditis elegans* to localized thermal stimuli," *BMC neuroscience*, vol. 14, no. 1, p. 66, 2013.

[22] B. Chong, Y. O. Aydin, G. Sartoretti, J. M. Rieser, C. Gong, H. Xing, H. Choset, and D. I. Goldman, "A hierarchical geometric framework to design locomotive gaits for highly articulated robots," in *Robotics: science and systems*, 2019.

[23] S. Ramasamy and R. L. Hatton, "Soap-bubble optimization of gaits," in *2016 IEEE 55th Conference on Decision and Control (CDC)*. IEEE, 2016, pp. 1056–1062.

[24] N. Cohen and J. H. Boyle, "Swimming at low reynolds number: a beginners guide to undulatory locomotion," *Contemporary Physics*, vol. 51, no. 2, pp. 103–123, 2010.